LEGIBILITY NOTICE

A major purpose of the Technical Information Center is to provide the broadest dissemination possible of information contained in DOE's Research and Development Reports to business, industry, the academic community, and federal, state and local governments.

Although a small portion of this report is not reproducible, it is being made available to expedite the availability of information on the research discussed herein.

DOE/ER/60082--T1

DOE/ER/60082--T1

DE84 005696

FINAL TECHNICAL REPORT

Interagency Agreement No: DE-AI01-82ER-60082

Three Dimensional Global Modeling of Atmospheric CO_2

I. Fung, J. Hansen, D. Rind

DISCLAIMER

NASA Goddard Space Flight Center
Institute for Space Studies
2880 Broadway
New York, NY 10025

1. Introduction

It seems likely that a great amount of information on the sources and sinks of atmospheric CO_2 is contained in the geographical, seasonal and interannual variations of the global atmospheric CO_2 distribution. The measured variations of CO_2 at several locations (Fig. 1) illustrate large variations in the amplitude and phase of seasonal change, as well as interannual variations, superimposed in an increasing secular trend. Recent analysis of the CO_2 records by Keeling and his collaborators (1982) reveal that the amplitude of the seasonal cycle has detectable interannual variations and may be increasing in time (Fig. 2). Keeling (1982) has also found that the meridional gradient of CO_2 in the atmosphere is also changing in time (Fig. 3).

We have initiated a modeling effort to study the prospects of extracting some of the potential information on CO_2 sources and sinks from observed CO_2 variations. The approach is to use a three-dimensional (3-D) global transport model, based on winds from a 3-D general circulation model (GCM), to advect CO_2 noninteractively, i.e., as a tracer, with specified sources and sinks of CO_2 at the surface. If the model can reproduce the general character of observed CO_2 variations on the basis of physically justified sources and sinks, it may then be used for experiments to determine the sensitivity of the global CO_2 distribution to various assumptions about CO_2 sources and sinks. It is anticipated that this approach may lead to useful quantitative limits on some CO_2 sources and sinks.

In the following we first identify the 3-D model employed in this study and then discuss biosphere, ocean and fossil fuel sources and sinks, including discussion of some preliminary tracer model results.

2. Tracer model

The tracer model uses winds generated from the GISS General Circulation Model (Hansen et al., 1983) to advect CO_2 as an inert trace constituent. While the GCM model II is able to reproduce the main features of the atmospheric circulation, the model deficiencies must be kept in mind in interpreting tracer experiments. The model resolution usually employed (8° latitude x 10° longitude), illustrated in Fig. 4, is sufficient to produce fairly realistic atmospheric longwaves and large scale eddies as occur at middle and high latitudes; it cannot, however, resolve the smaller scale tropical disturbances and this may affect transports at low latitudes. Also our understanding and modeling ability for many physical processes (Fig. 5) is rudimentary; accurate parameterization of moist convection may be especially important for simulating transports, but this process is presently treated in very simple ways in GCM's.

It is important to understand the limitations of the present 3-D modeling, discussed for example by Hansen et al. (1983), as these affect the ability to interpret observed characteristics of the global CO_2 distribution. However, we believe that it is appropriate to begin to do tracer experiments with existing 3-D modeling capability, because these experiments will be useful for helping to define model capabilities and deficiencies, thus aiding the process of 3-D model development.

Terrestrial Biosphere

Fung et al. (1983) have used a global vegetation map (Matthews, 1983) and simple ad-hoc definitions of CO_2 exchange between the biosphere and the atmosphere as input to the tracer model to study the geographical variation of the seasonal cycle of CO_2 in the atmosphere. The study demonstrates that large longitudinal variations exist in the atmospheric CO_2 distribution and that a 3-D approach is necessary for accurate analysis of the global carbon cycle.

We present here the results of three experiments with different biospheric CO_2 exchange functions. These functions are based on (1) Machta (1972), (2) Pearman and Hyson (1980), and (3) a global net primary productivity (NPP) map based on vegetation type to which Azevedo's (1982) seasonal CO_2 uptake and release curves were applied.

Experiment 1. Machta (1972) constructed a table of carbon exchange by month and 20° latitude belts based on information from Lieth (1965) and assumptions about seasons of growth and decay. For each month, we perform an area-weighted interpolation from Machta's 20° latitude zone to our model's ~8° latitude zone. The monthly carbon flux within each model belt is then uniformly distributed over the land areas in the zone.

Experiment 2. The Pearman and Hyson (PH) model consists of 20 equal-area zones for the surface of the globe. By requiring their model simulated CO_2 distributions to match those observed, PH obtained values of CO_2 flux for each month and each of their model zones. We assume that PH's monthly fluxes are evenly distributed over land within their zones. In order to equivalence PH's equal-area zones to the tracer model's latitude belts, we use a weighting by continental area and interpolate their fluxes to the model's latitude belts. The monthly carbon flux within each belt of the tracer model is again uniformly distributed over land area in the belt.

Experiment 3. Using about 90 sources, Matthews (1983) constructed a global, 1° x 1° resolution vegetation file containing about 200 vegetation types. Annual NPP values are assigned to each vegetation type in each 1° x 1° cell and the resultant NPP map at the model resolution is shown in Figure 6. The global NPP value is 45 x 10^{12} kg C/yr.

Azevedo (1982) constructed simple curves of CO_2 uptake and release by the biosphere. These curves are based loosely on the assumption that uptake and release are governed by air and soil temperatures and that these processes are turned off when temperatures fall below some critical value. They are illustrated in Figure 7. From 40°N to 70°N, biospheric uptake of CO_2 is concentrated in the months of May to August, while release occurs throughout the year but with maxima in the same months. From 10°N to 40°N, release occurs uniformly throughout the year while maximum uptake occurs from May to August. Like Machta (1972), Azevedo assumes that from 10°N to 10°S, uptake and release overlap throughout the year, resulting in zero net seasonal exchange. Azevedo shifts the curves by 6 months for the southern hemisphere.

In this experiment we combined the NPP map with Azevedo's carbon uptake and release curves to form the monthly flux of carbon to the atmosphere:

$$\text{SOURCE}(\lambda,\theta,t) = \text{NPP}(\lambda,\theta) \times [\text{RELEASE}(\theta,t) - \text{UPTAKE}(\theta,t)]$$

The UPTAKE and RELEASE curves are normalized so that

$$\sum_{1\ year} \text{RELEASE}(\theta,t) = \sum_{1\ year} \text{UPTAKE}(\theta,t) = 1$$

or that no net annual exchange of carbon occurs. Note that this exchange, like the NPP, possesses both latitudinal and longitudinal variations even with these extremely simple seasonal distributions.

The tracer model with these biospheric sources/sinks was run for 25 months until the annual cycles repeated themselves. The CO_2 concentrations are defined relative to a globally uniform (and arbitrary) background concentration, so that a positive (or negative) R (CO_2 mole fraction means that the simulated concentration is greater (or less) than the background.

The seasonal oscillations of CO_2 concentrations simulated at grid boxes corresponding to five observation sites are shown in Figure 8 together with the observed annual cycles as cited by PH and Bolin and Bischof (1970). As one would expect from the magnitudes of the source functions in the three experiments, the peak-to-peak amplitudes of the CO_2 oscillations at these locations increase from experiments 1 to 3. Machta's biospheric exchange function underestimates the amplitudes, as has been noted by other investigators (Pearman and Hyson, 1980; Azevedo, 1982). In experiment 1, the underestimation is about 50% at Mauna Loa and 63% at Point Barrow. PH's source functions, constructed to duplicate the observations with their model, produce a peak-to-peak amplitude of 6.0 ppm at Mauna Loa, close to that observed. However, the amplitudes at Papa and Barrow are underestimated by about 45%. In experiment 3, the amplitudes simulated at the grid boxes of Point Barrow and at Mauna Loa are within 10% of those observed. The amplitude at OWS Papa is underestimated in all three experiments even thought the amplitudes at the land stations are reasonably simulated in experiment 3.

The phase of the CO_2 annual cycles at station locations can be seen in Figure 8. In all three experiments the months of predicted maxima and minima at the station locations are within 2 months of those observed. However, the simulated annual cycles at the northern stations, especially at Point Barrow, lack the asymmetry seen in the observed cycles. This is probably because we have assumed, even at 70°N, that the growing season starts in May instead of in early June, when the snow melts at this latitude.

The azonal nature of the CO_2 distributions is apparent in Figure 9, which shows the seasonal amplitudes at the surface as simulated in experiment 3. Except in the northern hemisphere tropics which is relatively well-mixed zonally, the isopleths of amplitude closely parallel the coastlines. The highly productive and seasonal land vegetation and, in this experiment, the absence of oceanic source/sinks create large contrasts in CO_2 concentration between land and sea. These contrasts are not smoothed effectively by the wind. The amplitudes simulated over ocean are only half the maximum amplitudes simulated over land at similar latitudes. The isopleths tighten and wrap the coastlines more closely at higher latitudes as land biomes become more strongly seasonal. Amplitudes greater than 20 ppm are seen in the boreal forests of North America and Siberia. In South America, Azevedo's seasonality applied to the rain forests south of 10°S results in an amplitude of 10 ppm. Validation of model results in these regions is presently impossible because of the

limited observations of CO_2 in the atmosphere.

Figure 10 shows the surface concentrations of CO_2 simulated in experiment 3 for the month of August, the end of the growing season at mid-latitudes in the northern hemisphere. The diversity of vegetation types over land and the lack of CO_2 exchange over the oceans produce longitudinal gradients as large as 4ppm over 20° longitude at ~50°N. In general, isopleths of CO_2 concentration at the surface closely follow the trajectories of the surface wind (cf. Figure 10, lower part). This can be easily seen in the southern hemisphere tropics. The southeasterly trades sweep CO_2 off the continents, creating tongues of CO_2 downwind. In the northern hemisphere tropics, in the rising branch of the Hadley circulation, the relatively small amplitude of CO_2 exchange with the terrestrial biosphere and very effective vertical mixing by convection create a small contrast in CO_2 concentration between land and sea. This contrast is further reduced by the steady easterly winds, resulting in small longitudinal gradients. The dynamics is reversed at mid-latitudes in the northern hemisphere. The net biospheric flux of CO_2 is large over a percentage of the surface area in a latitude belt, and vertical mixing is weak except under storm systems. The persistent cyclonic and anticyclonic wind systems transport CO_2 along a meandering path around the latitude circle. The zonal surface wind speed simulated by the GCM is < 5 m/s at these latitudes. This implies that the time scale for zonal mixing, about 2-3 months at 45°N, is longer than the time scale for the source/sink (about a month) and zonal homogeneity is never achieved.

Of the three biospheric exchange functions investigated, that of experiment 3, constructed from a global NPP map and Azevedo's (1982) seasonal exchange curves, produces CO_2 annual cycles at locations of monitoring stations most similar to those observed. In this exchange function, the net flux of carbon to the biosphere during the growing season (i.e., the GSNF) is 10.7×10^{12} kg C in the northern hemisphere and 2.3×10^{12} kg C in the southern hemisphere. The GSNF estimate for ~45°N to 90°N is 7.7×10^{12} kg C, which is larger than PH's estimate of 2.5×10^{12} kg C and Bolin and Keeling's (1963) estimate of 4.1×10^{12} kg C for the same region. These biospheric exchange functions, when input to the respective models, all reproduce reasonably well the amplitudes of the observed CO_2 cycles. However, only one tracer transport model and one biospheric exchange function can be correct. The differences in GSNF thus underlie the need for an ecological model of CO_2 exchange rather than one based on model requirements.

Analysis of the zonal mean balance in the lower troposphere confirms the dominant role played by the total meridional transport in the redistribution of CO_2 within each hemisphere. Eddy transport is diffusive, while mean meridional transport is in the direction of the mean meridional winds and may therefore be countergradient. At mid-latitudes, convergence of total meridional transport alters by 50% or more the signal from local biospheric exchange. In April, in particular, the transport processes at mid-latitudes nearly cancel the local biospheric input, resulting in a near-zero concentration tendency. This suggests that year-to-year variations of the CO_2 concentration at the monitoring stations may result from internal variability of the atmospheric circulation. Information about changes in the biosphere can be deduced only from concurrent changes in CO_2 concentration at several stations whose natural variability is understood.

It may be fortuitous that a simple biospheric exchange function such as used in experiment 3 closely reproduces the annual cycles at several coastal monitoring stations. However, the experiment underestimates the amplitude at OWS Papa and predicts amplitudes as large as 25 ppm in the northern hemisphere boreal forests. The mid-latitudes in the northern hemisphere is shown to be a region with large biospheric source/sink, incomplete zonal mixing, and possibly the greatest sensitivity to changes in atmospheric circulation and/or sources/sinks. Annual oscillations of sea surface temperatures at these latitudes have peak-to-peak amplitudes of ~10°C. Indeed GEOSECS measurements have revealed amplitudes of ~50 ppm in oscillations of oceanic pCO_2 in the Sargasso Sea (Takahashi et al., 1980). These seasonal changes in the upper ocean may thus have a significant, albeit small, effect on the annual cycles of atmospheric CO_2. The sparsity of CO_2 monitoring sites at present places a great reliance on model calculations to deduce information about the sources and sinks of CO_2. While an ecological model of the terrestrial biosphere is imperative for understanding the role of the biosphere in the atmospheric CO_2 cycle, the influence of the oceans on the annual cycle of CO_2 must not be overlooked.

Ocean

The observed seasonal cycles of sea surface temperature give rise to large seasonal oscillations in oceanic pCO_2 (Weiss et al., 1982). The atmospheric response to such oscillations in oceanic pCO_2 has been investigated with the tracer model coupled to the upper ocean. Temperature dependent carbon chemistry (Takahashi, 1976) is included in the mixed layer. Fig. 11 shows the amplitude of the seasonal cycle of atmospheric CO_2 thus induced. As is expected, this cycle is small compared to that induced by exchange with the terrestrial biosphere. Nonetheless, the amplitude at the observing sites are about 10% or more of those observed; the phasing is opposite that resulting from biospheric exchange. Hence, in order to infer information about the activities of the terrestrial biosphere and about changes in these activities, the oceanic contribution to the seasonal cycle should not be neglected.

Fossil fuels

The temporal and spatial distribution of anthropogenic CO_2 release is fairly well known (Rotty, 1982). It is not likely that study of atmospheric CO_2 will improve quantification of the anthropogenic source. However, in order to interpret observed atmospheric CO_2 changes, it is necessary to include the fossil fuel source in the model, or at least to subtract the secular trend from the observations.

Discussion

The initial attempts to model the atmospheric CO_2 distribution, including couplings to the ocean and biosphere as sources and sinks of atmospheric CO_2, encourage the notion that this approach will lead to useful quantitative constraints on CO_2 fluxes. Realization of this objective will require:

1) Continued improvement in the realism of the global transport modeling. Model development should proceed in concert with tracer studies, including CO_2 and other constituents, because such studies can contribute substantially to

understanding of key model deficiencies and thus to the improvement of the models.

2) Extended timeline of atmospheric CO_2 monitoring, with improved precision and improved definition of the uncertainties in the measured CO_2 amounts. Many of the potential applications depend upon measurement of perturbations of the CO_2 distribution, changes in time or in geographic distribution, and hence accurate calibration and intercalibration among different observing stations is important.

3) Given an accurate knowledge of model capabilities and limitations and given a good understanding of CO_2 observations and their limitation, there is a need for good ideas concerning what quantitative information on the carbon cycle can be inferred from global modeling. Potential examples:

A) It may be possible to determine information on the global distribution of NPP, if the seasonality of CO_2 uptake and release can be well defined on the basis of vegetation type and climate. Fig. 12 suggests the plausibility of relationships between climate parameters and CO_2 uptake and release by vegetation.

B) Detectable interannual variations of photosynthetic uptake, illustrated at a specific location in Fig. 13, may exist on a larger scale. If relationships between droughts and the atmospheric CO_2 distribution can be determined, it would provide valuable information on the terrestrial biospheric source of CO_2.

C) Can El Nino and other sea surface temperature anomalies (Fig. 14) be related to observed changes in atmospheric CO_2? This could provide a useful check on our understanding of the ocean chemistry portion of the carbon cycle. If this is well in hand, it may be possible to relate deviations between modeled and observed ocean CO_2 to ocean plant productivity.

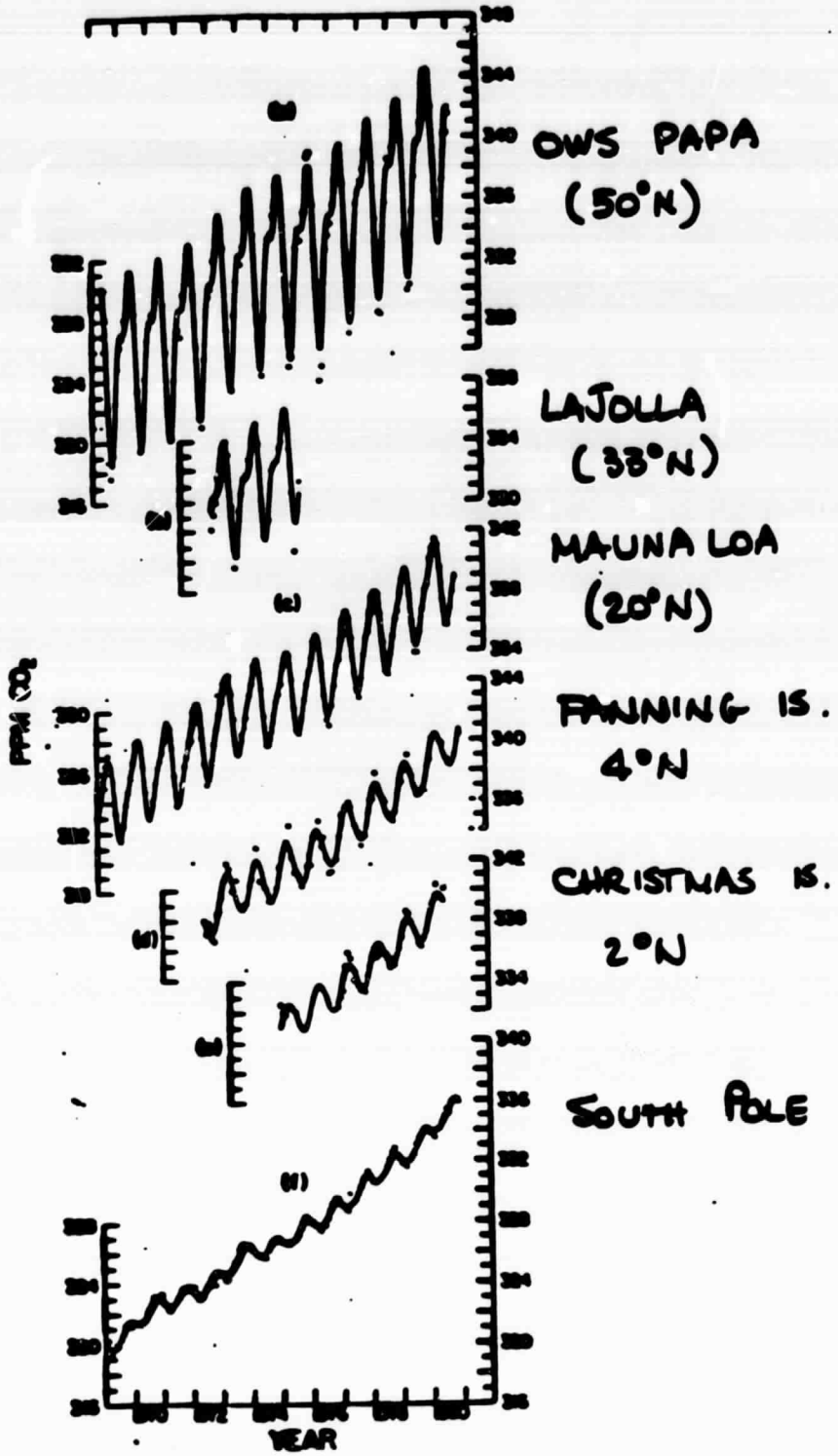

Figure 1. CO_2 trends observed at several stations, based on data of Keeling et al.

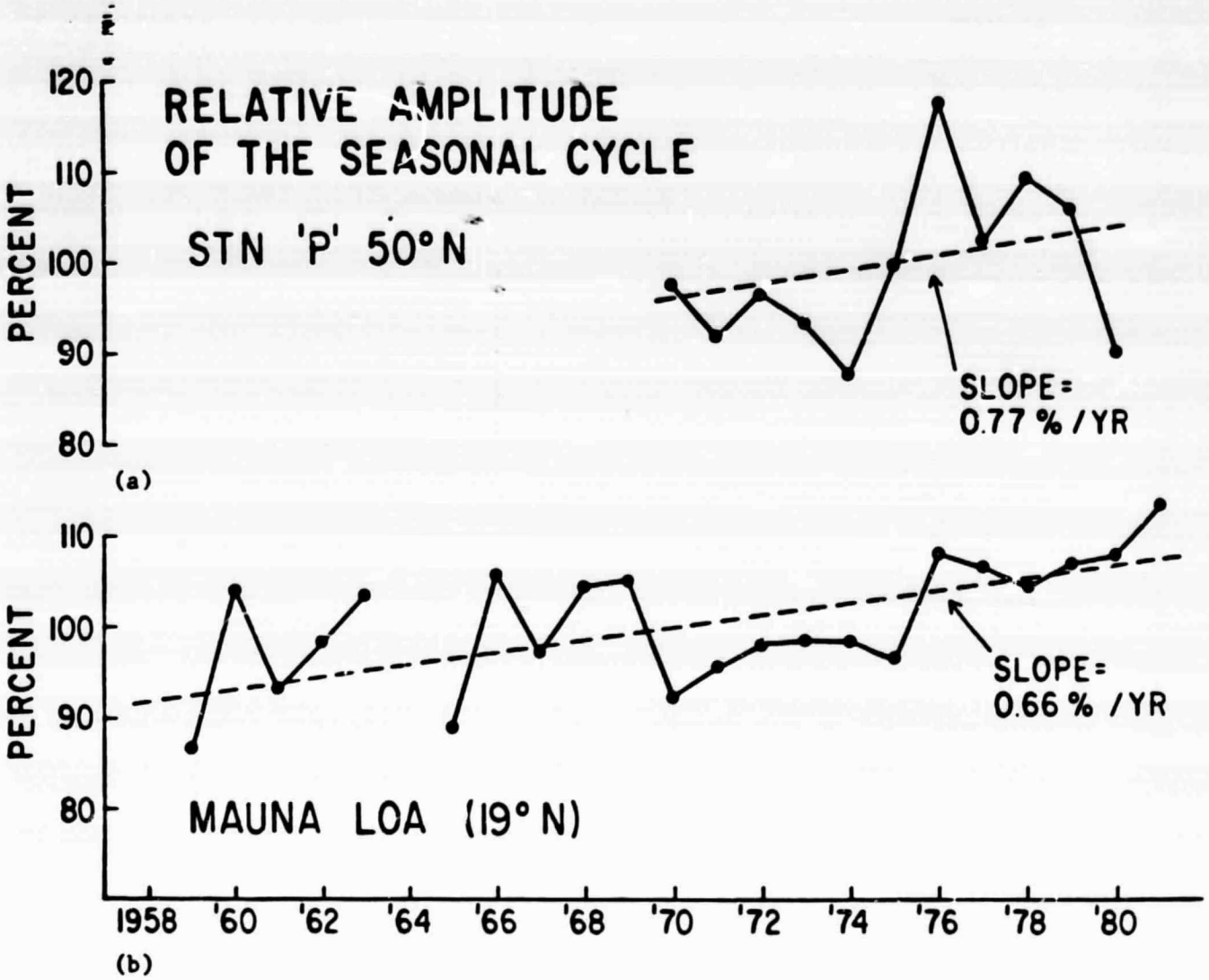

Figure 2. Interannual variation of the seasonal amplitude of atmospheric CO_2 concentration at a) Papa and at b) Mauna Loa (from Keeling, 1982). The mean seasonal amplitude is ~12 ppm at Papa and ~6 ppm at Mauna Loa.

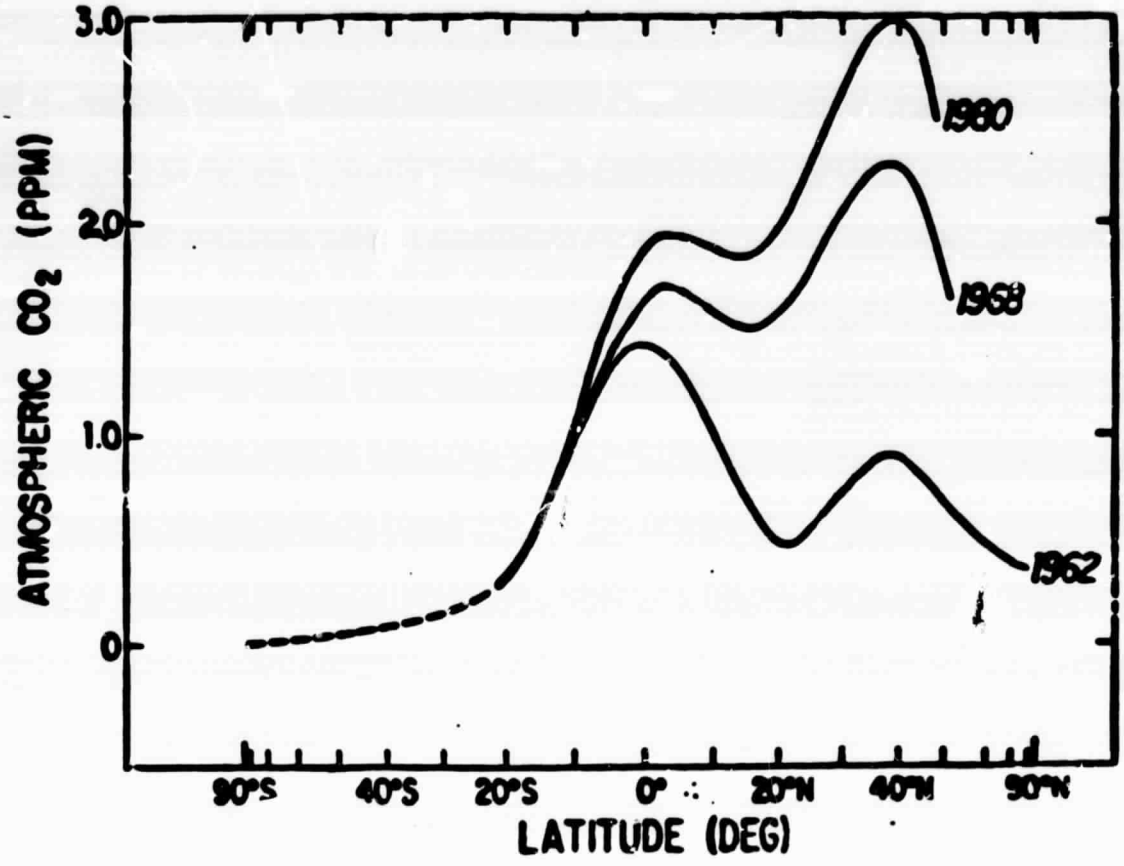

Figure 3. North-South variation in the mean annual concentration of atmospheric CO_2 for 1962, 1968 and 1980 (from Keeling, 1982).

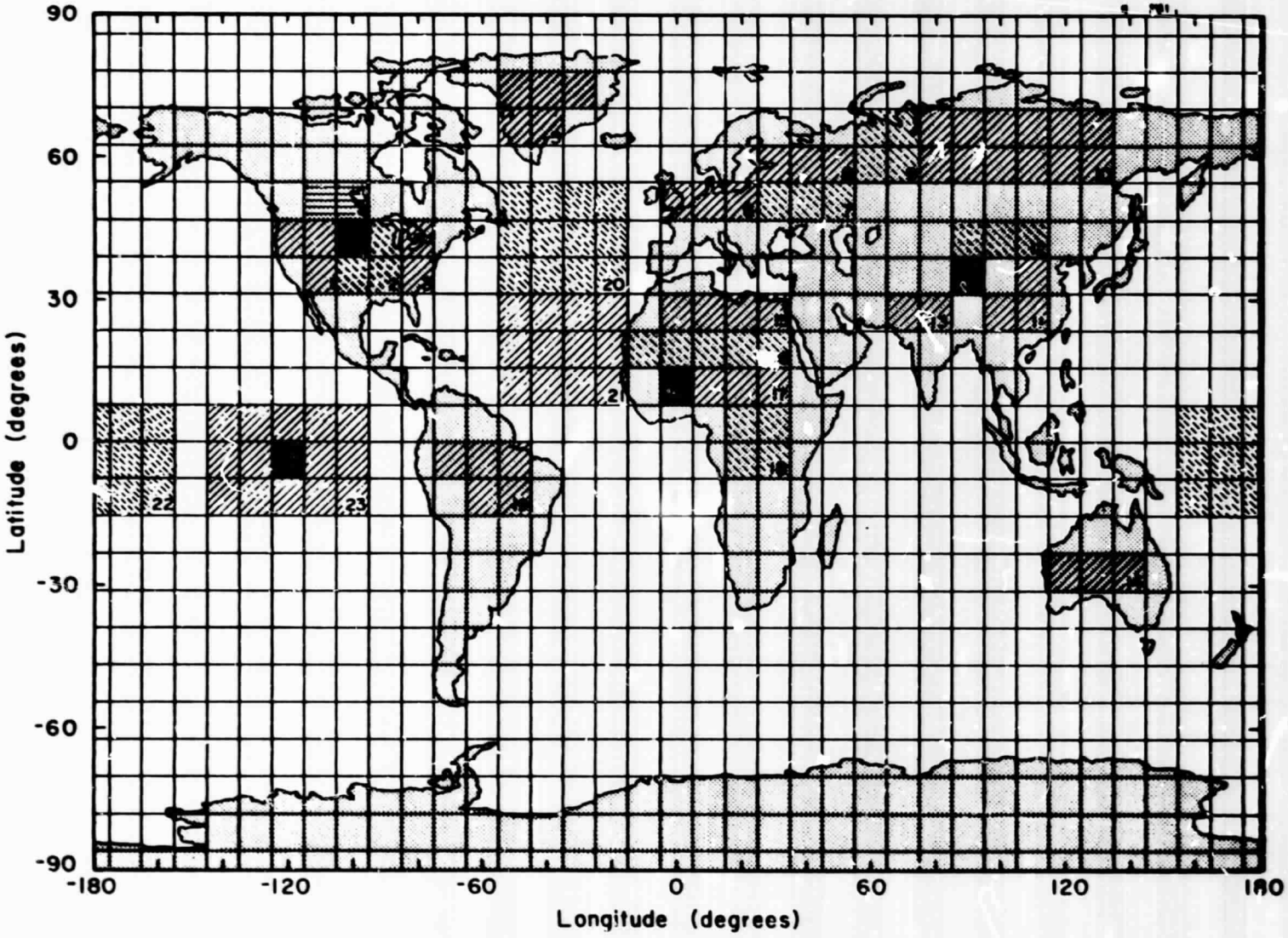

Figure 4. Grid spacing for 8° x 10° model.

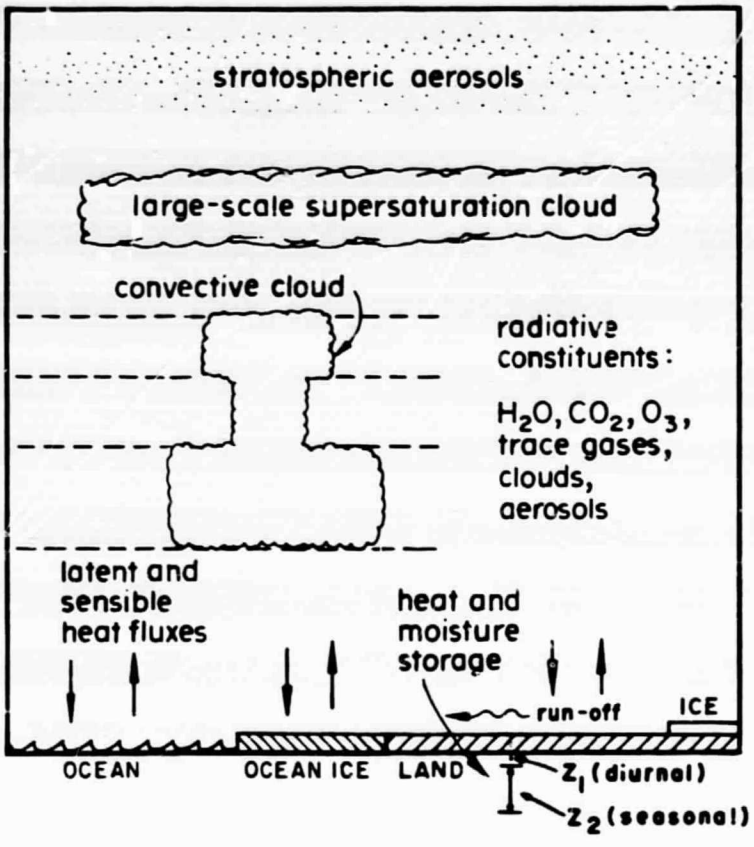

Figure 5. Schematic illustration of model processes at a single gridbox.

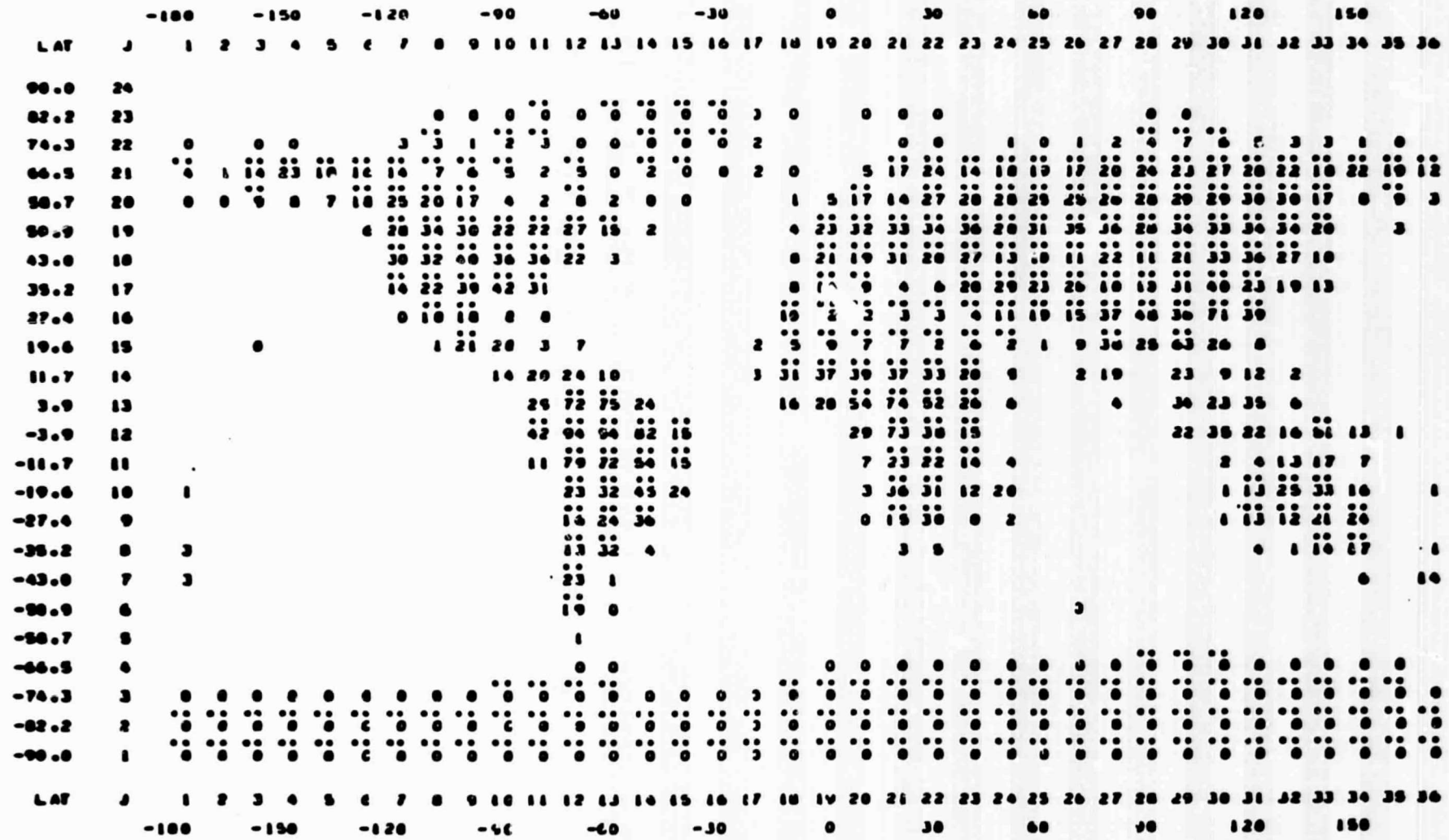

Figure 6. Assumed global distribution of NPP (x 10 gm C/m^2/yr) at the tracer model resolution.

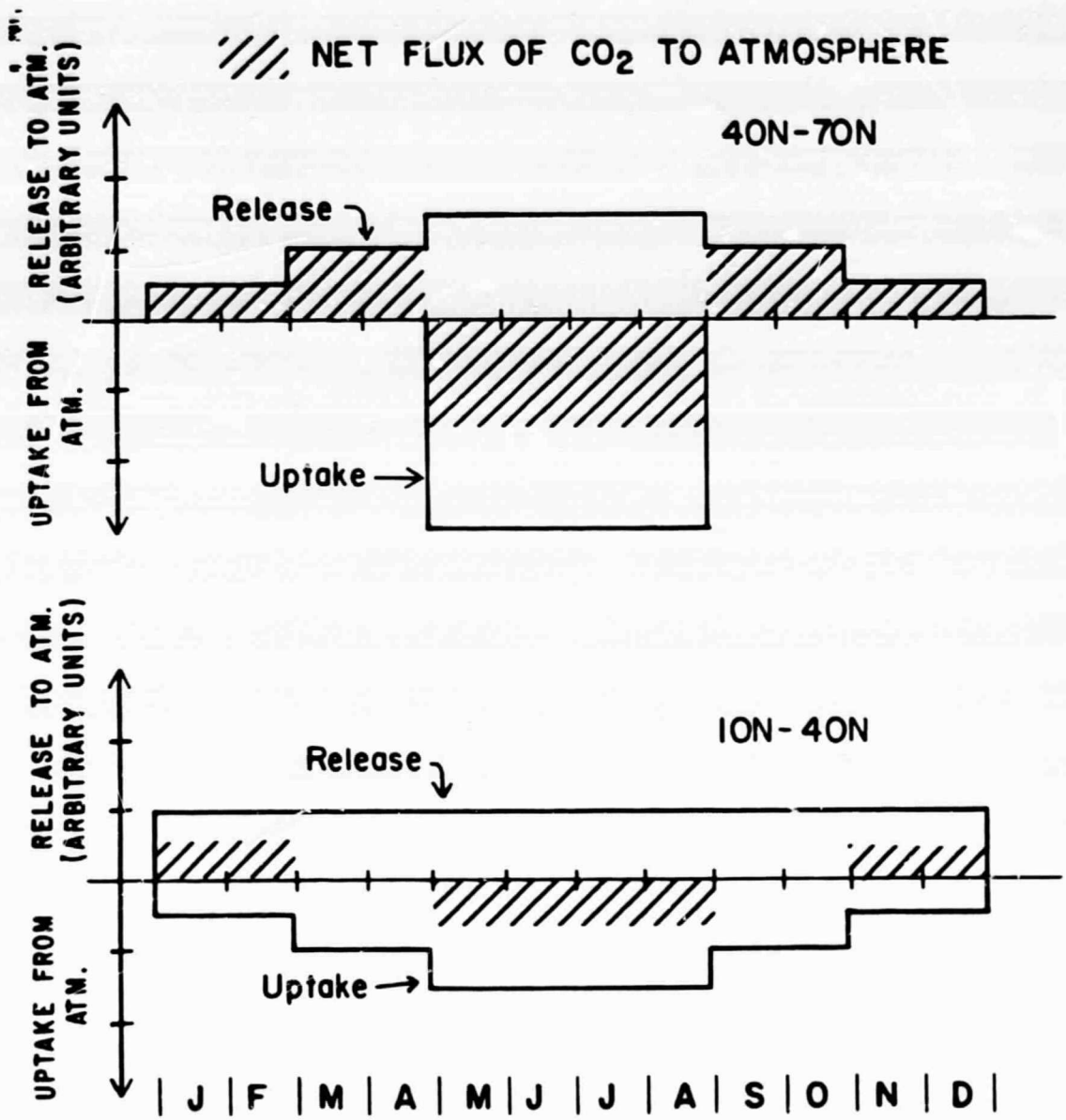

Figure 7. Seasonality of biospheric uptake and release of CO_2 (after Azevedo, 1983) employed in experiment 3.

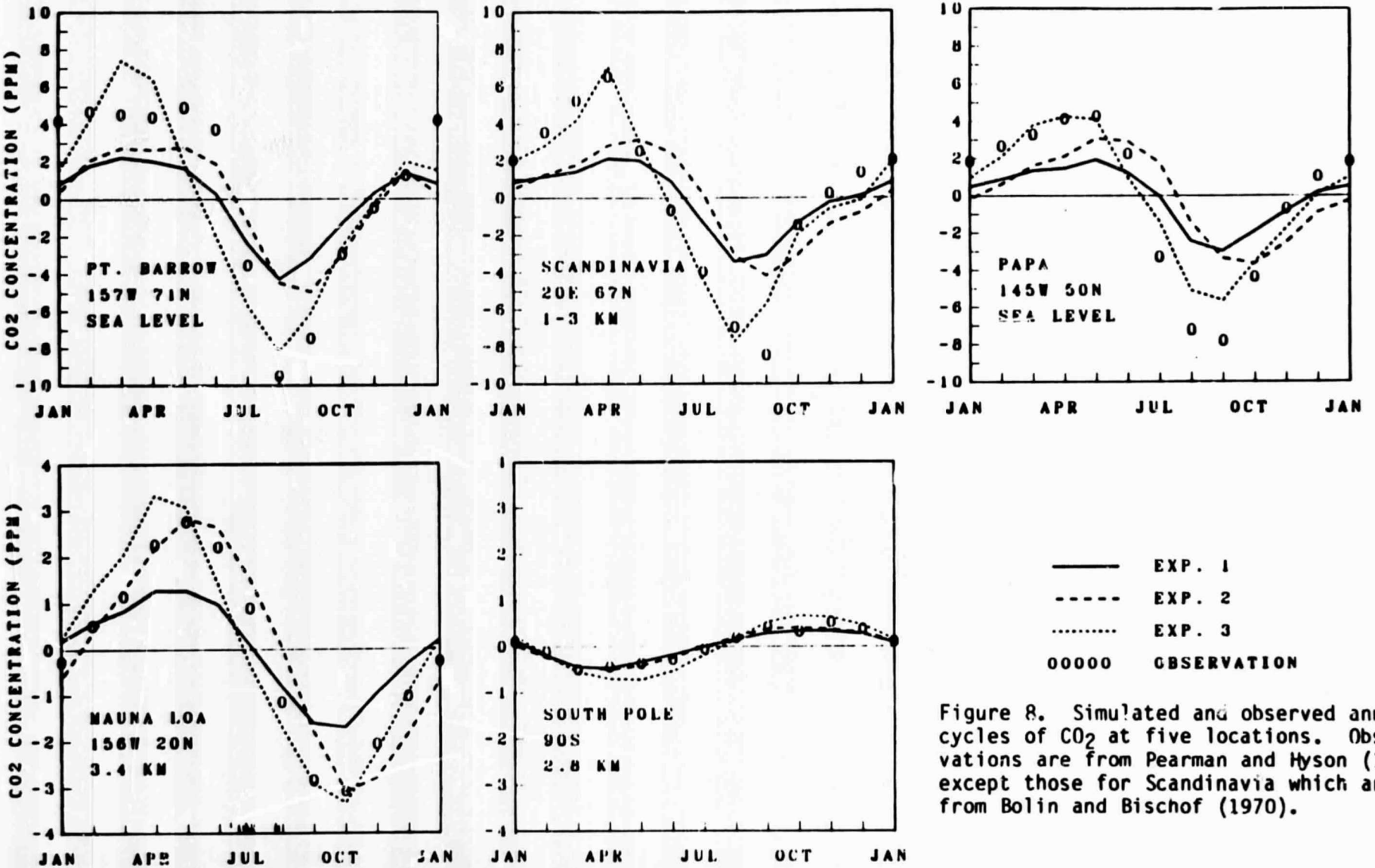

Figure 8. Simulated and observed annual cycles of CO_2 at five locations. Observations are from Pearman and Hyson (1980), except those for Scandinavia which are from Bolin and Bischof (1970).

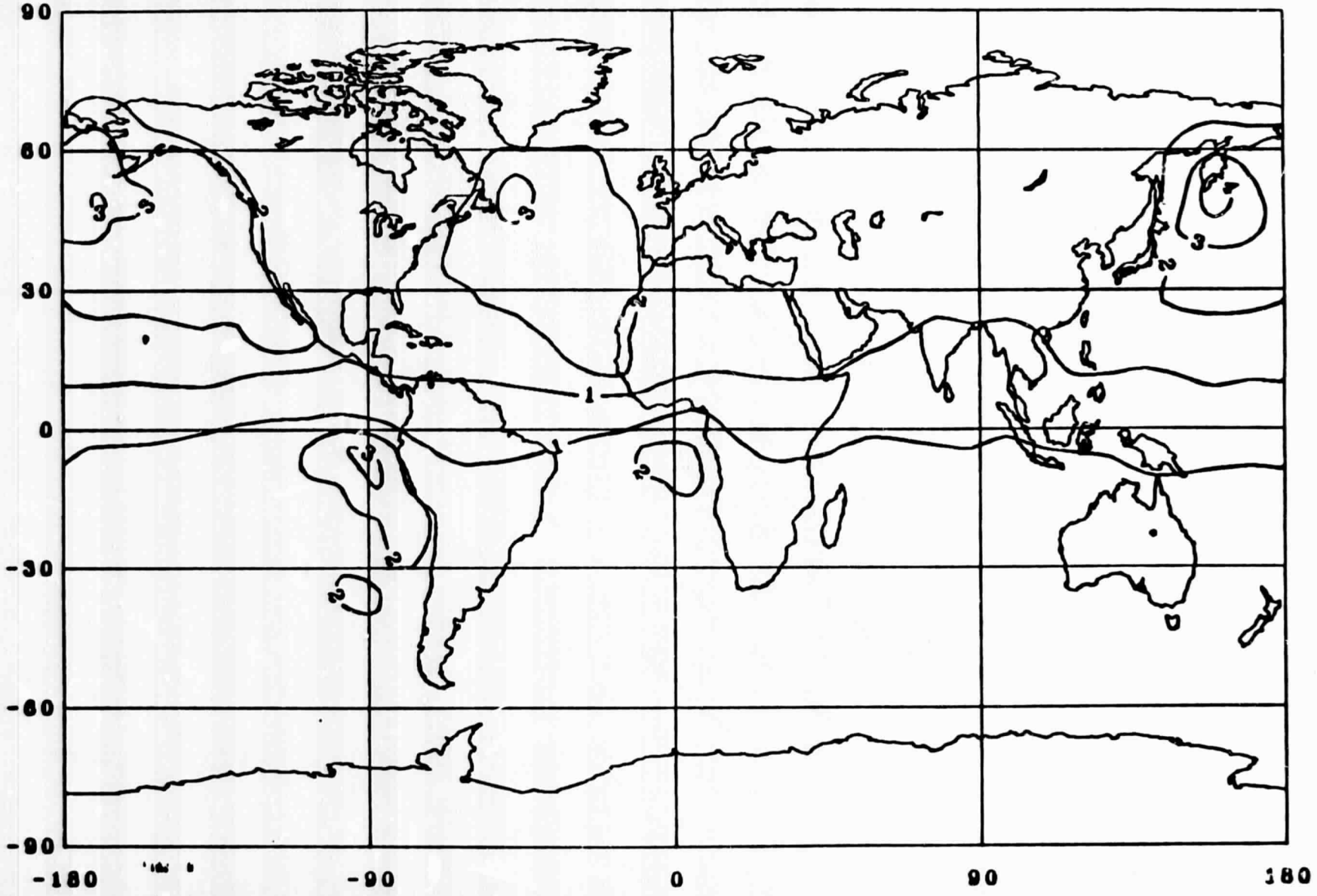

Figure 9. Peak-to-valley amplitude (ppm) of seasonal surface CO_2 variation, as simulated in experiment 3.

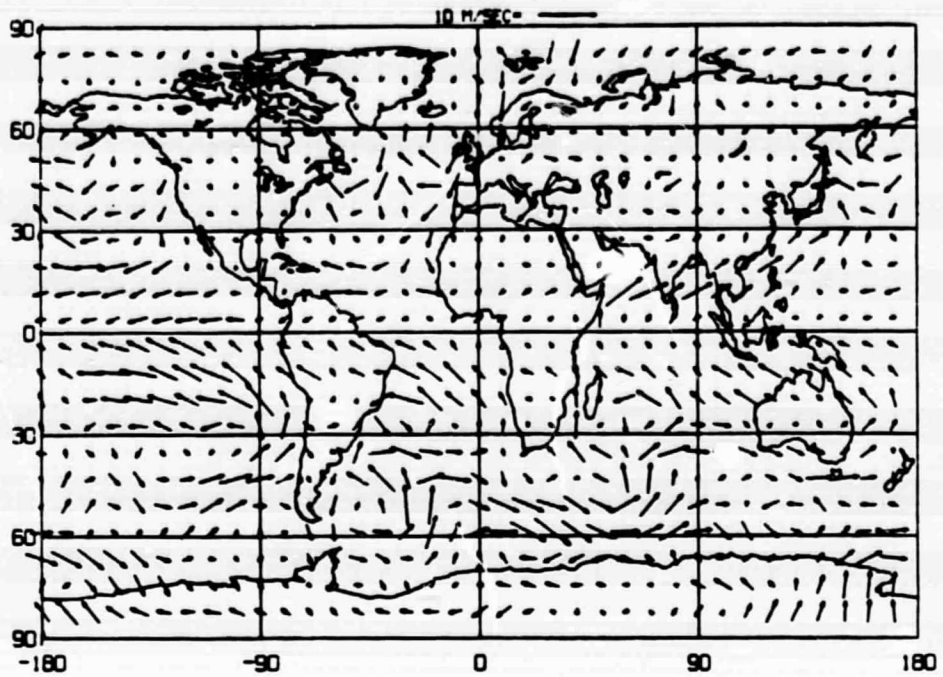

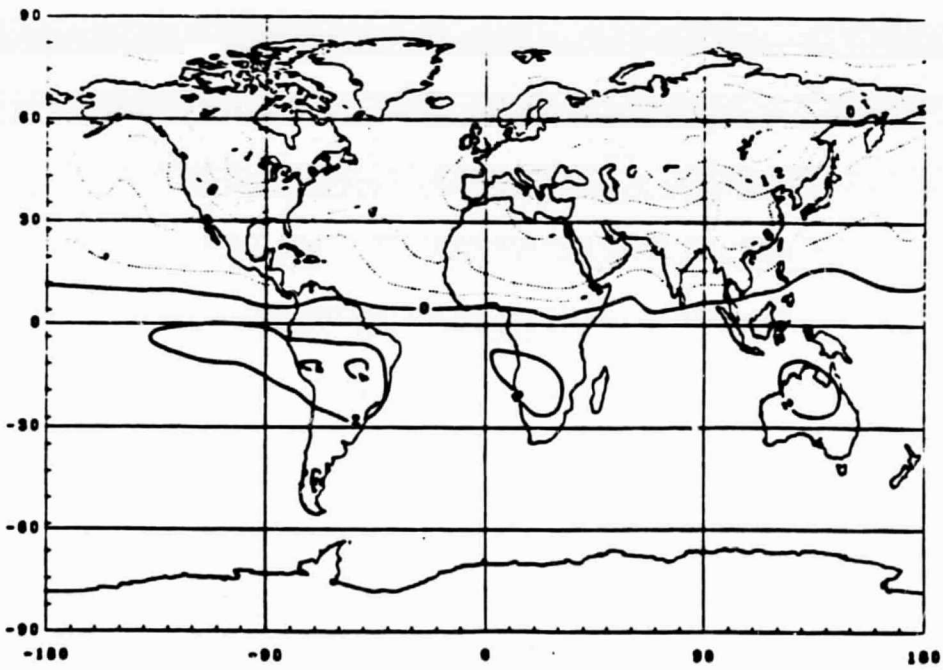

Figure 10. August surface winds in model II (upper) and August surface CO_2 perturbation (ppm) as simulated in experiment 3.

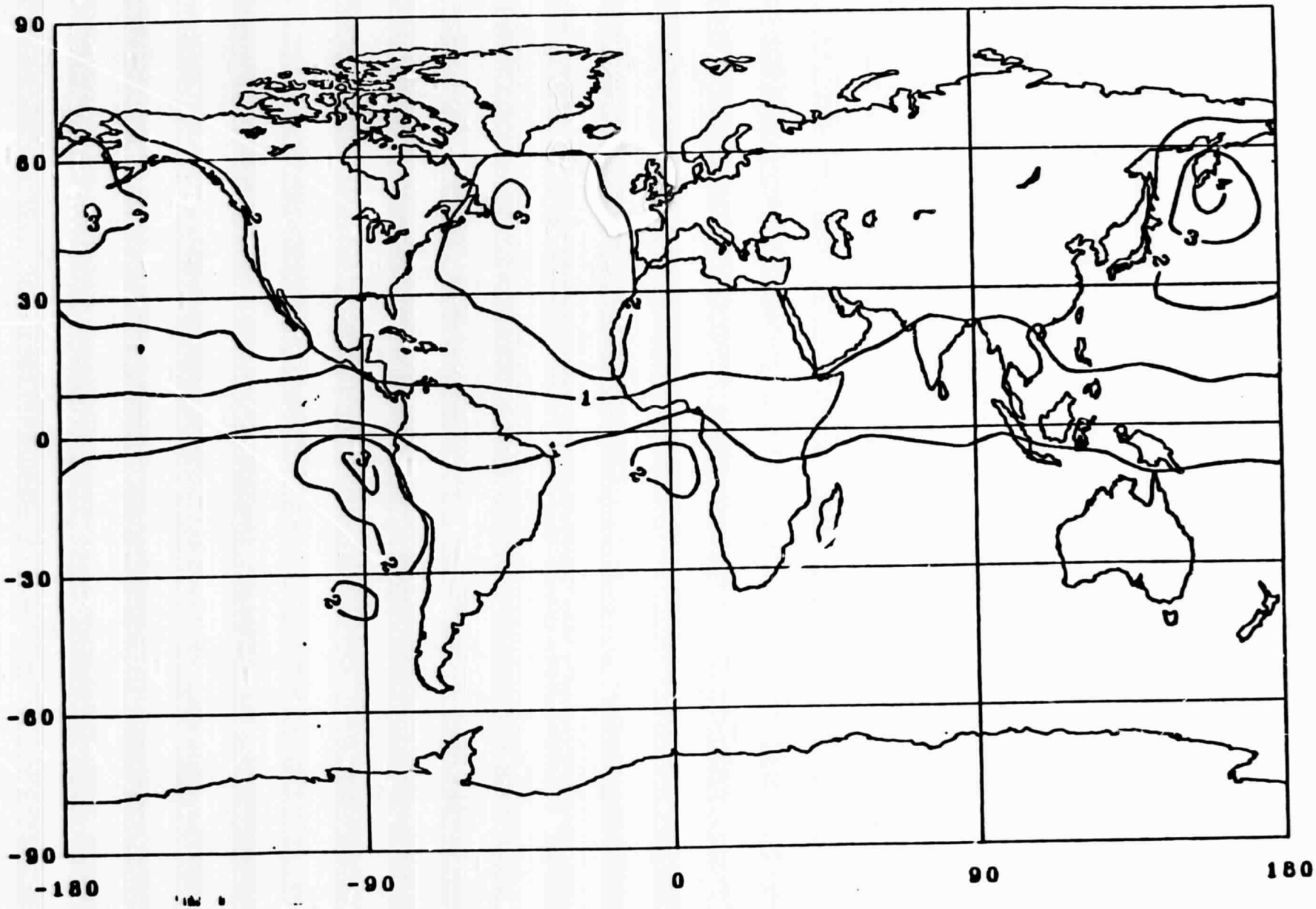

Figure 11. Model-simulated peak-to-peak amplitude (ppm) of surface atmospheric CO_2 response to temperature-induced pCO_2 oscillations in the surface waters.

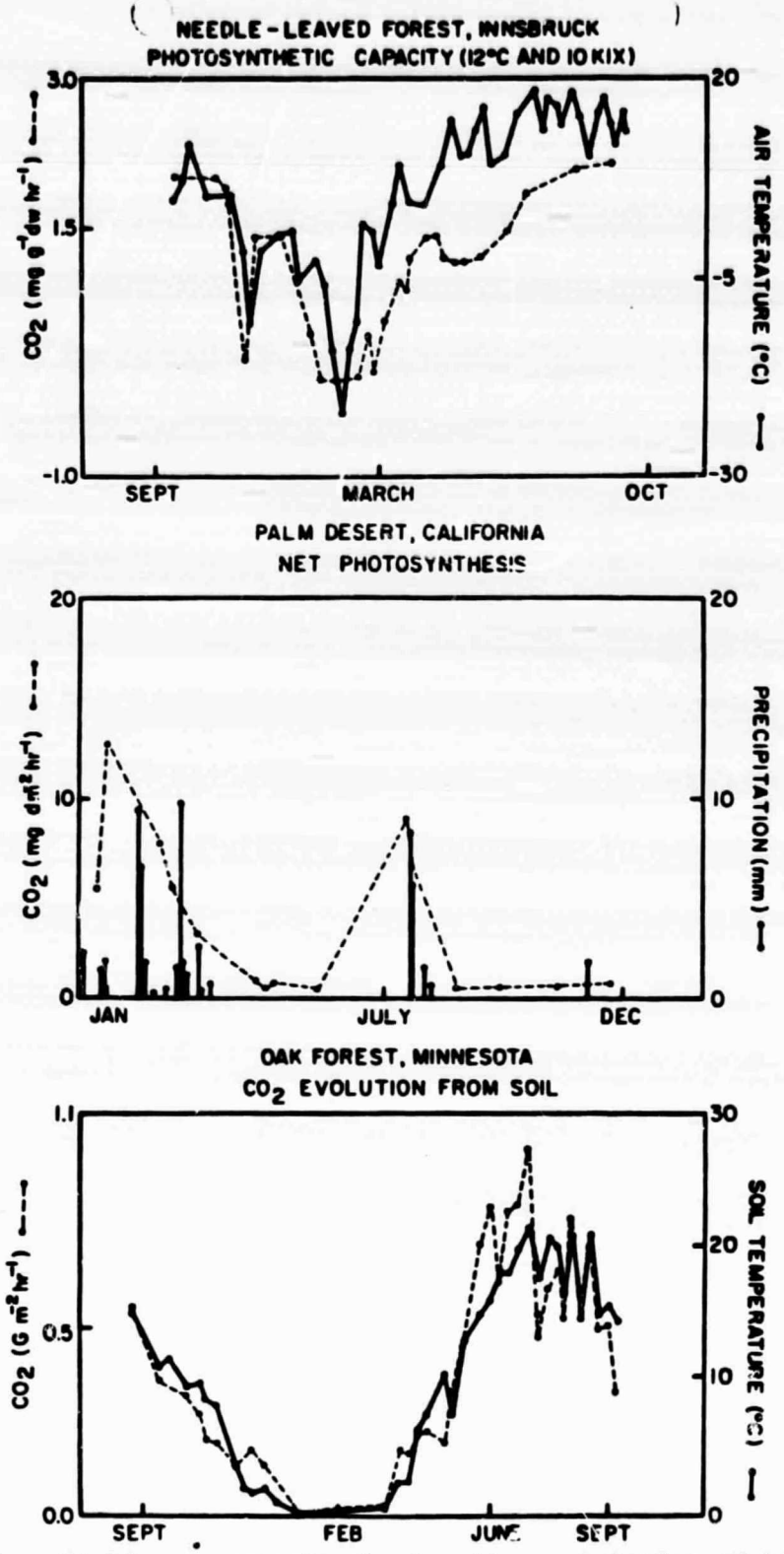

Figure 12. Some field measurements showing the covariation of biospheric carbon uptake and release with ambient temperature and precipitation. (a) shows the photosynthetic capacity of sun shoots of a mature spruce and the surface air temperature in Innsbruck, Austria (from Tranquilini, 1979 and Larcher, 1981). (b) shows the net photosynthesis of opunta basilaris in Palm Desert, California and the precipitation events at the site (from Szarek and Ting, 1974). Opunta basilaris is a CAM plant adapted to dry arid environments. An enhanced level of CO_2 assimiliation persists during periods of rainfall. (c) shows the CO_2 evolution rates from the soil and the soil temperature measured in an oak forest in Anoka, Minnesota (from Reiners, 1968).

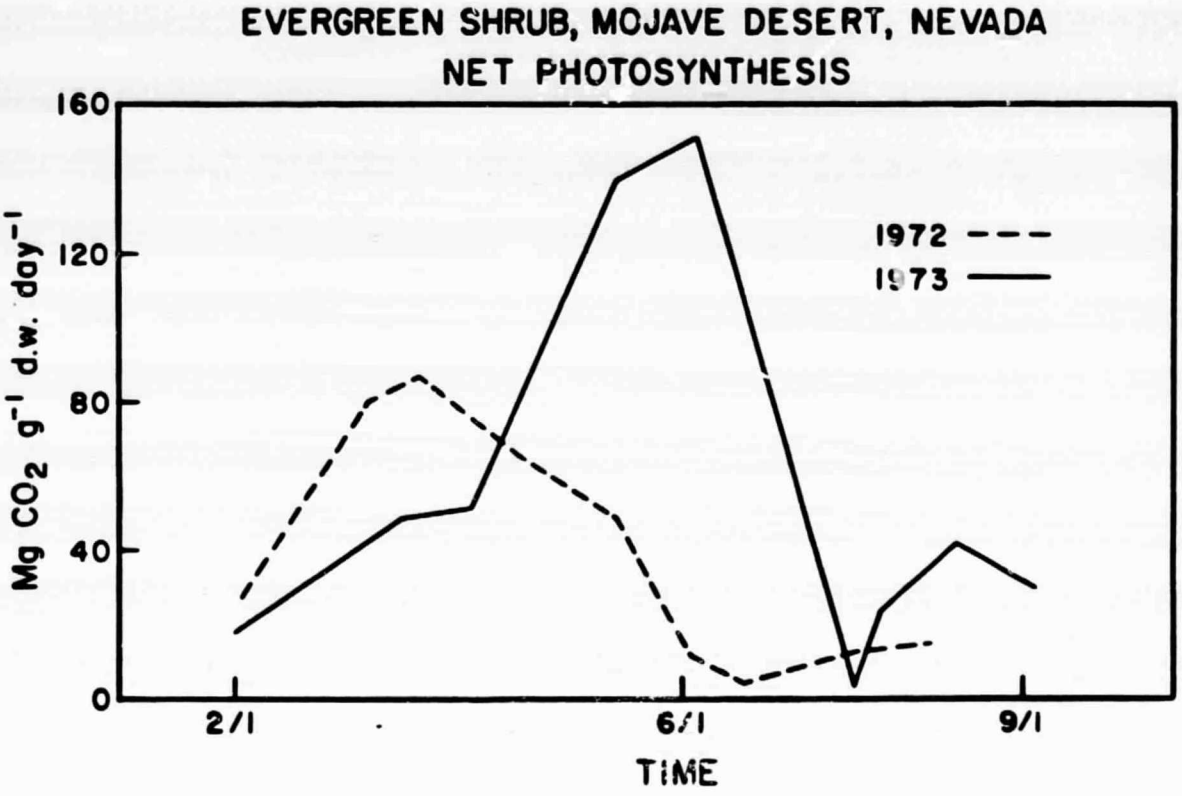

Figure 13. Net photosynthetic uptake of CO_2 by an evergreen shrub in the Mojave Desert for 1972 and 1973 (after Bamberg et al., 1976).

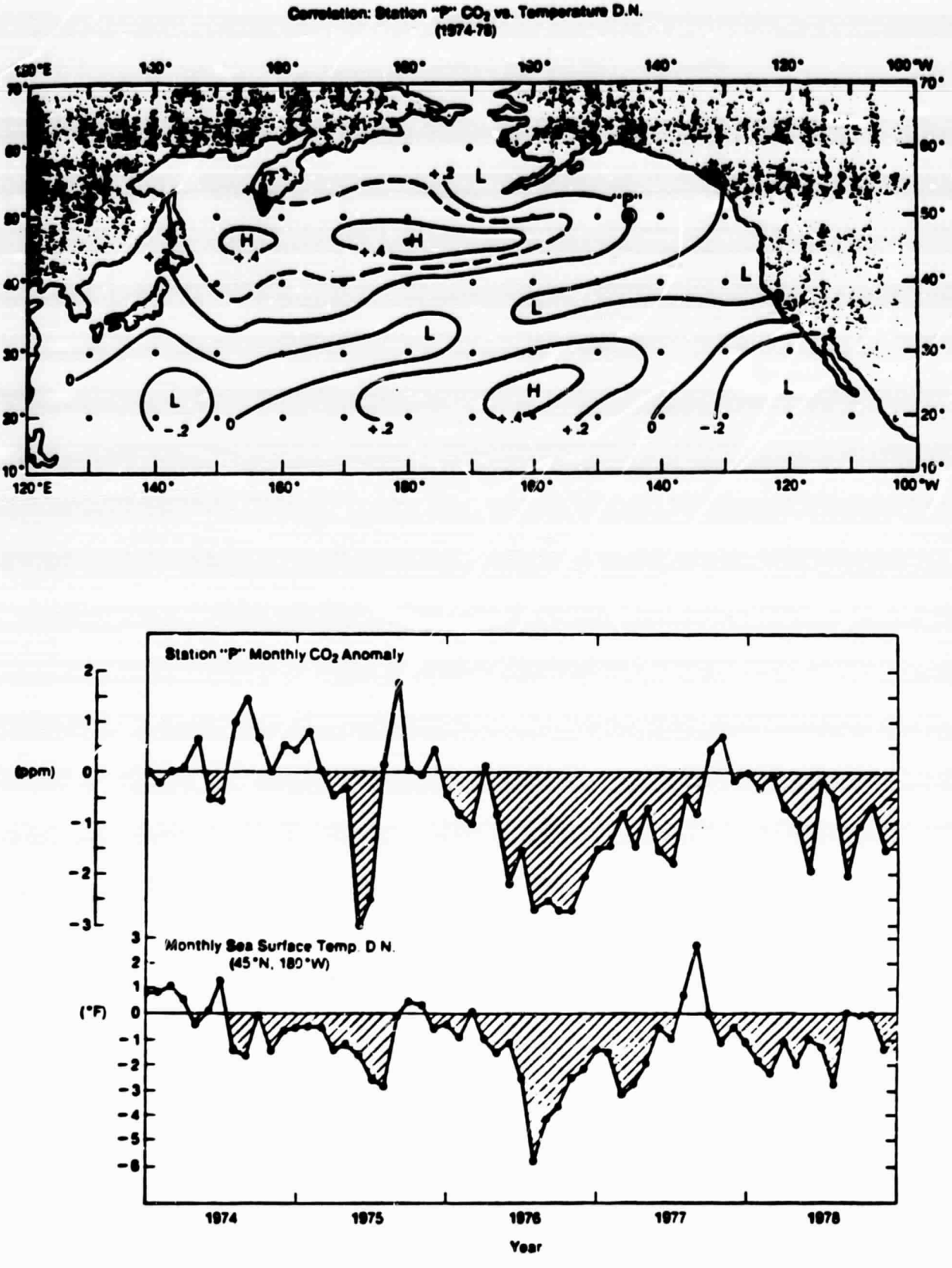

Figure 14. a) Correlations of stations pCO_2 anomalies with SST anomalies for 1974-1978. b) CO_2 anomalies at Station P and SST anomalies at 45°N, 180°W (from Hansen et al., 1981).